International Journal of Chemical Sciences

Research | Vol 16 Iss 2

Part-II-New Advanced Synthesis for High Performance Anti-Corrosive Lubricants of some Selected Inorganic Pigments II-2D and 3D-Nanostructural Features of Laser Assisted Anatase Phase TiO_2

Elsabawy KM[1,2*], Refat MS[1,3] and Fallatah AM[1]

[1]Department of Chemistry, Taif University, 888-Taif, Saudi Arabia

[2]Department of Chemistry, Tanta University, Tanta-31725, Egypt

[3]Department of Chemistry, Port Said University, Port Fouad, Egypt

[*]**Corresponding author:** Elsabawy KM, Department of Chemistry, Faculty of Science, Taif University, 888-Taif, Saudi Arabia, Tel: +966-127272020; E-mail: khaledelsabawy@yahoo.com

Received: March 27, 2018; **Accepted:** April 11, 2018; **Published:** April 14, 2018

Abstract

Advanced solution route was successfully applied to synthesize nano-anatase. Ultrahigh energy He-Ag-Laser (224.3 *nm*) irradiations coupled with sonication were applied for the 1st time as grains sizes splitter (promoter to lower sizes). The present investigations managed to introduce thermally-stable anatase TiO_2 with ultrahigh BET surface area (789 m^2g^{-1}). Ti(IV)-tetra iso-propoxide (TTIP) was applied as precursor for synthesizing nano-TiO_2. The produced gel (HO-Ti-O-Ti-O-Ti-OH)n was divided into two equal portions one as blank and other one forwarded to sonication/laser irradiations treatments by time dose equal to ~10 min. of laser irradiations per hour of sonication. Finally produced irradiated Gel dried in oven at 130°C followed by microwave assist to avoid any solvent tracer and finally sintered at 560°C for 4 h. The produced Ti(IV) oxide was carefully investigated and well characterized by Raman spectra, XRD, SEM and 3D-AFM.

***Keywords:* Solution Route; Anatase-TiO2; XRD; 3D-AFM; He-Ag-Laser; Sonication**

Introduction

Titanium dioxide (TiO_2) has many forms as nano-structured oxide and incorporated in many of technological, industrial applications as white colorant pigments, semiconductors, catalysis and electrochemical sensors due to their unique physical and structural features. The functional behavior of the produced TiO_2 is strongly impacted and controlled by applied conditions of preparation, the size, orientations, morphology and crystalline form of the particles.

Citation: Elsabawya KM, Refata MS, Fallataha AM. Part-II-New Advanced Synthesis for High Performance Anti-Corrosive Lubricants of some Selected Inorganic Pigments II-2D and 3D-Nanostructural Features of Laser Assisted Anatase Phase TiO_2. Int J Chem Sci. 2018;16(2):259

The main efficient approach used to manufacture TiO_2 is wet (liquid-phase) including all solution routes chemistry. Wet methods exhibit some control of the particle size and its pores, but the crystalline phase can be amorphous and contain impurities [1]. Flame synthesis methods enable continuous operation and produce a high purity product [2,3]. It is well known that TiO_2 occurs in nature in three distinct crystallographic phases: anatase, rutile and brookite. While anatase TiO_2 are the most widely used as photo-catalysts for oxidative decomposition of organic moieties and an excellent photo-catalyst for photodecomposition and solar-energy conversion due to its high photo-reactivity [4].

Anatase TiO_2 has many advantages as cheapness, non-toxicity and non-corrosive material in addition to its excellent functionality and long term thermal stability. The structural and micro-structural features of titanium oxide have been researched [2-9]. The main problem connected with these trials was that the growth of TiO_2 nano-crystallites takes a long time. Therefore, it is highly desirable to find some new advanced routes and techniques that are capable of overcoming the above problems to prepare TiO_2 in short time with reasonable purity. Many attempts have been made in this field over the past few years [10-19].

The major goals of the present investigations are:

- Application for the 1st time ultrahigh energy He-Ag-laser irradiations plus sonication as TiO_2-grains splitter to lower gains size regardless what is the approach applied in the synthesis of anatas TiO_2.
- Synthesizing of ultra-high BET nano-TiO_2 in short time with simple eco-technique.
- Trying to control particle morphology and size.

Experimental

Synthesis of TiO_2 Nano-particles

Nano-structured particles of TiO_2 have been synthesized with the sol-gel method from the hydrolysis of two different titanium precursor. This process normally proceeds *via* an acid-catalyzed hydrolysis step of titanium (IV) alkoxide/or hydroxylated titanium followed by condensation process.

The development of Ti-O-Ti chains is favored with low content of water, low hydrolysis rates and excess titanium alkoxide in the reaction mixture. Titanium tetra isopropoxide (TTIP) was applied as a precursor and mixed with (HNO_3/ethanol mixture) with stirring for 1 h, at pH range of (1-1.5). After that 20 ml of deionized water was added to the above mixture and stirred for 3 h at room temperature. Sonication step was performed for 6 h then finally the solution was dried at 130°C for 20 min. followed by microwave assisted to avoid solvent tracers.

The thermal treatment of produced precursor gives titanium oxide with different bi-products according to applied temperatures as reported in [20,21].

$Ti(OC_3H_7)4 \rightarrow TiO_2+4C_3H_6+2H_2O$……..……...……Temp.≥ 400°C..... (1)

$Ti(OC_3H_7)4 \rightarrow TiO_2+2C_3H_6+2C_3H_7OH$…….….Temp. ≤ 400°C…….. (2)

Sonication and helium-silver laser irradiations process

The vessel containing Ti-O-Ti chains during gel formation of TiO_2 nano-particle was subjected to be target for both ultrasonicated source and He-Ag-laser irradiations as described in FIG. 1.

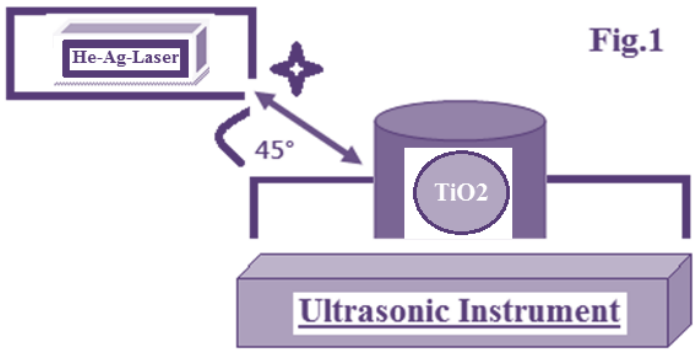

FIG. 1. **Sonication process coupled with ultrahigh energy He-Ag-Laser irradiation at distance 3 cm with angle 45° to TiO_2-sample during gel/hydroxylated oxide formation with power 103 W/cm^2.**

The samples were irradiated by three different doses 1, 2 and 3 h from ultrahigh energy He-Ag-Laser with power of 103 W/cm^2 at distance of 3 cm by angle 45° respectively. The applied He-Ag Laser has the following specifications; the laser output is insensitive to ambient temperature and requires no warm-up or other preheating and no temperature regulation. The laser head and power supply are designed for operation at an average input power of 120 W/cm^2 in order to keep the system air cooled and simple. In order to provide the discharge conditions needed for optimum output (12 A at 350V=4.2 kW). The focal length F of the focusing lens, D is the beam diameter (5.5 mm) and λ is the laser wavelength (224.3 nm). Therefore, this laser can be focused to 5 μm spot on sample with a 5.5 mm focal length. The energies of applied He-Ag Laser were sufficient to melt homogeneously the surface and near surface layers. SEM and AFM were used for monitoring morphological changes. Ultrasonic bath was SU-27TH which has an output power of 300 watts, frequency of 28 kHz and 500 watts heater was used in this study.

Characterizations and structural measurements: Atomic force microscopy (AFM): High-resolution Atomic Force Microscopy (AFM) is used for testing morphological features and topological map (Veeco-di Innova Model-2009-AFM-USA). The applied mode was tapping non-contacting mode. Scanning Electron Microscopy (SEM): Scanning electron microscopy measurements were carried out by using a computerized SEM with elemental analyzer unit (Philips-USA). Raman Spectra Measurements: was performed *via* raman spectrometer (T64000 HORIBA Jobin Yvon) using a 50 mW and 514.5 nm wavelength Ar-green laser. The X-ray diffraction (XRD): X-ray diffraction measurements were carried out at room temperature on the ground samples using Cu-Kα radiation source and a computerized Shimadzu (Japan) diffraction meter with two theta scan technique.

Surface area calculations (BET): Brunauer–Emmet–Teller (BET) specific surface areas (SSA) were obtained with an automatic system (Model 2200A, Micro-meritics Instrument Co., Norcross, GA), using nitrogen gas as an adsorbate at

liquid nitrogen temperature. The pore size distribution calculated from the desorption branch of the nitrogen isotherm by the BJH (Barrett-Joyner-Halenda) model.

Results and Discussion

Structural Identification and Raman spectra

FIG. 1 (a, b) displays XRD profile patterns recorded for tetragonal anatase phase sintered at 560°C for the two different precursors (assisted laser/sonication and non-assisted). The fingers print peaks for two patterns are nearly identical with little displacements reveal to experimental conditions differences.

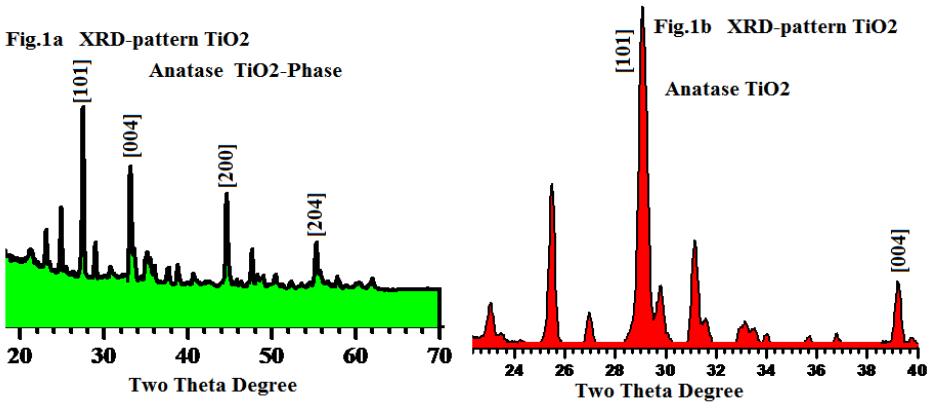

FIG. 1 (a, b): **XRD patterns recorded for TiO_2 resulted from applied two precursors routes.**

The analysis of X-ray powder diffraction patterns FIG. 1a and 1b indicated by presence of tetragonal anatase phase TiO_2 with I41/amd space group (FIG. 2). The evaluated lattice parameters of tetragonal TiO_2 phase were found $a=b=3.7390$Å and $c=9.3786$ Å respectively, which are in full agreement with those reported in [8-11]. The analyses of XRD peak positions as shown in FIG. 1a and 1b display small shift in the main peak locations within narrow range ~ ± 3° in the two theta values due to experimental conditions differences which is attributable to that the gel precursors were exposure to two different treatments.

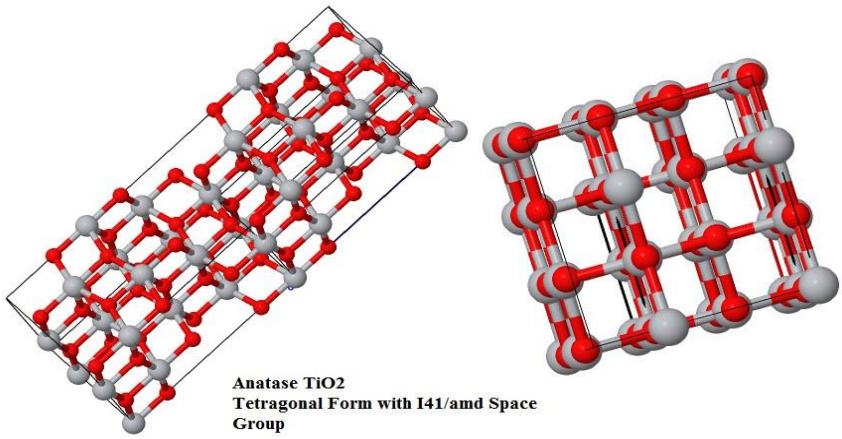

FIG. 2. **Crystal structure image of Anatase-Tetragonal phase.**

From FIG. 1a and b one can notify that peaks appear at 2θ values 26.2, 33.4, 44.3 and 54° are corresponds to the crystal planes of [101], [004], [200] and [204] respectively with narrow shift in contrast with those reported in literatures [12-14]. The particles sizes averages were evaluated from SEM, AFM-particles size analyzer and also calculated using Debye-Scherrer's formula using XRD patterns and found in the range of 8 to 41 nm which is fully consistent and matched with literatures as [6-9].

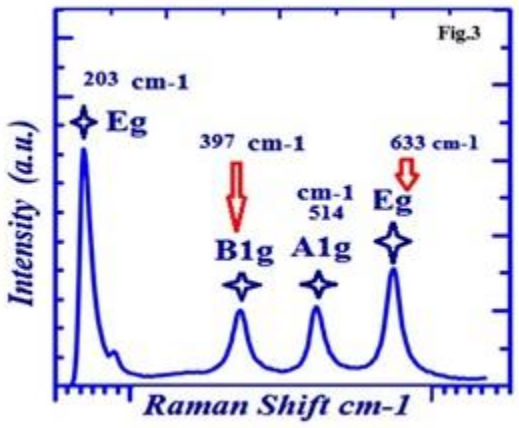

FIG. 3. **Raman spectra measured for synthesized meso-porous Anatase-TiO_2.**

FIG. 3 displays the main four characteristics Raman active modes of anatase tetragonal TiO_2 phase namely; B1g (397 cm^{-1}), A1g (514 cm^{-1}) and 2 Eg (203,633 cm^{-1}) respectively. The observed bands locations of Raman active modes were in full agreement with literatures [22-26]. The measured Raman spectra are matched with Park et al. [27] who reported that the tetragonal anatase structure is consisting of conventional cell of two primitive one, each with two TiO_2 units produced six active modes which are A1g (517 cm^{-1}), 2B1g (397 cm^{-1}, 517 cm^{-1}) and 3Eg (144 cm^{-1}, 197 cm^{-1} and 640 cm^{-1}) are Raman active [27]. The narrow shifts (± 7 cm^{-1}) in bands locations between present data and reference [27] are due to that Raman active modes are experimental conditions dependent.

Microstrurtural features

3D-Nano-and micro-structural features of resulted sol-gel precursor before sintering at 560°C, anatase TiO_2-without laser irradiations/sonication treatments and treated anatase TiO_2 were carefully investigated by both of AFM-and SEM as shown in FIG. 4 (a-c).

The particles sizes averages were evaluated from SEM, AFM-particles size analyzer and calculated also by using Debye-Scherrer"s formula and found in the range of 8 to 41 nm which is fully consistent with literatures [6-9]. FIG. 4a shows 3D-AFM and SE-micrograph images of sol-gel precursor before sintering at 560°C, it was observed that surface topology of the precursor is divided into two partitions with unified arrays with heights average ~ 0.45 µm. SE-micrograph of sol-gel precursor emphasized that most of grains aggregate as spherical unit shapes with relatively high diameter average ~ 6.3 µm due to swelling phenomena resulted from solvation effects of hydroxides groups.

FIG. 4b exhibits 3D-AFM and SEM images for pre-treated anatase TiO_2. One can conclude that surface topology in AFM-image has uniform homogeneous arrays with average heights of ~0.4 µm and fractions from particle sizes were ranged in between 23-41 nm. FIG. 4c displays 3D-AFM and SEM micrographs for treated mesoporous-anatase TiO_2. It can be seen that

surface arrays were arranged in good orders without violation under thermal effects of laser/sonication treatments with heights average of ~ 0.25 µm.

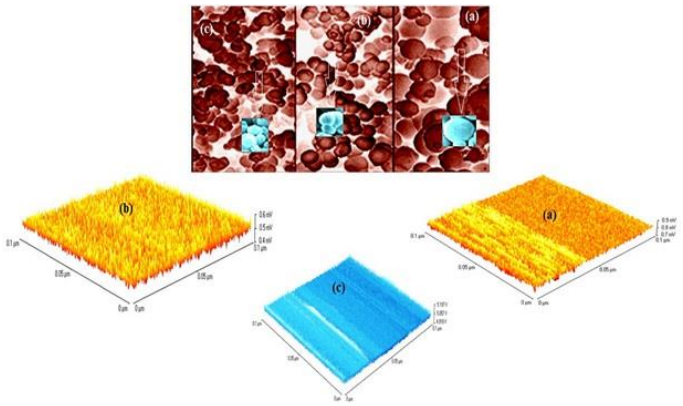

FIG. 4. **(a-c) 3D-AFM-images and SE-micrographs captured for: a) Sol-gel Precursor before sintering at 560°C, b) Anatase TiO_2-resulted without laser irradiations/Sonication process, c) Anatase TiO_2-resulted after laser irradiations/sonication assisted process.**

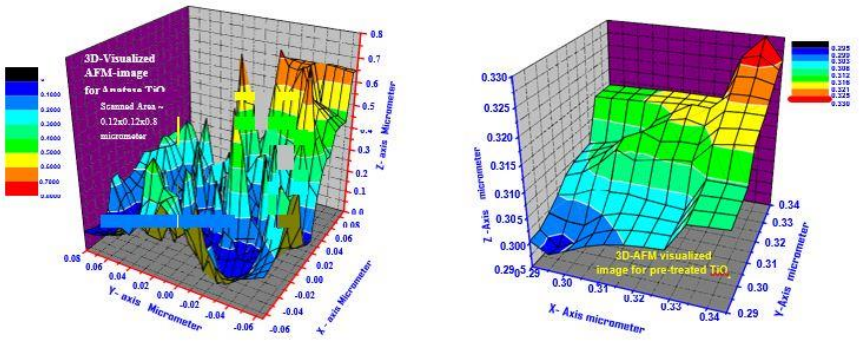

FIG. 5. **(a) 3D-AFM-visualized image applying non-contact mode for TiO_2 surface engineered *via* He-Ag laser/Sonication assist process for narrow scanned area 0.12 × 0.12 × 0.8 µm, (b) 3D-AFM-visualized image applying non-contact mode for pre-treated TiO_2 process for narrow scanned area 0.05 × 0.05 × 0.04 µm.**

The particles sizes averages of laser-treated anatase TiO_2 were carefully estimated *via* SEM and AFM-particles sizes analyzer and found in between 8-24 nm. This result emphasized the efficiency of laser/sonication as grains promoter to lower particle sizes and hence lower grains. For accurate mapping of the surface topology of laser-treated and pre-treated anatase TiO_2. The measured AFM-raw data were forwarded to the Origin-Lab version 6-USA program to visualize more accurate three-dimension surface of the anatase TiO_2 sample as shown in FIG. 5a and 5b. This process is new trend to get high resolution 3D-surface mapping with ultrahigh-resolution and give the possibilities of measuring narrow scanned area [28-30].

Analyses of FIG. 5a and 5b indicated by the following facts that support and reinforce the point of view that laser-treated-TiO_2 has ultrahigh BET surface area of 789 m^2g^{-1} (as clear in FIG. 5a surface topology with sharp heights) while pre-treated anatase TiO_2 has low BET surface area ~ 71 m^2g^{-1}.

The dimensions of scanned area in FIG. 5a were 0.12 × 0.12 × 0.8 µm, maximum heights observed was 0.8 µm (red zones) less than ~ 5%, minimum heights of ≤ 0.1 µm less than 1% represented by black color zones. From FIG. 5a, it can be seen that more than ~ 66% of heights gradient lies in the blue-zones with maximum heights of 0.4 µm while only 34% of scanned area have heights higher than 0.4 µm. These observations confirm the success of laser/sonication treatment as grains splitter and hence producing of ultrahigh surface area.

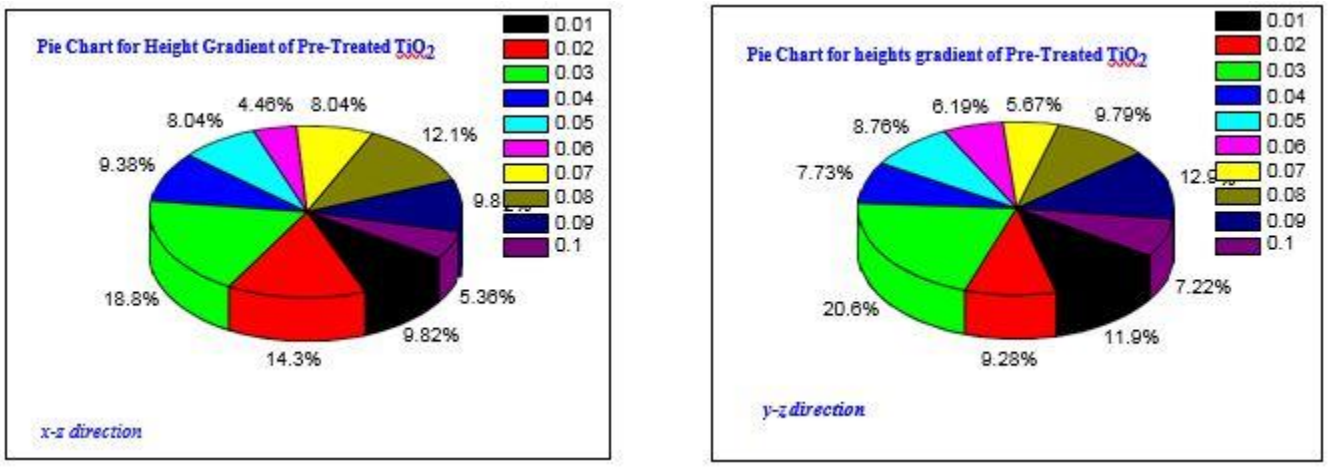

FIG. 6. **2D-AFM histograms through (xz, yz) for TiO_2-without Laser/Sonication treatments.**

FIG. 6a and 6b is showing heights gradient through xz, yz axes for pre-treated anatase TiO_2, as it clear the fractions of heights higher than 10 nm is the majority with ratio ~88%, those with heights ranged in between 10-42 nm while heights lower than 10 nm can be represented by only 12%.

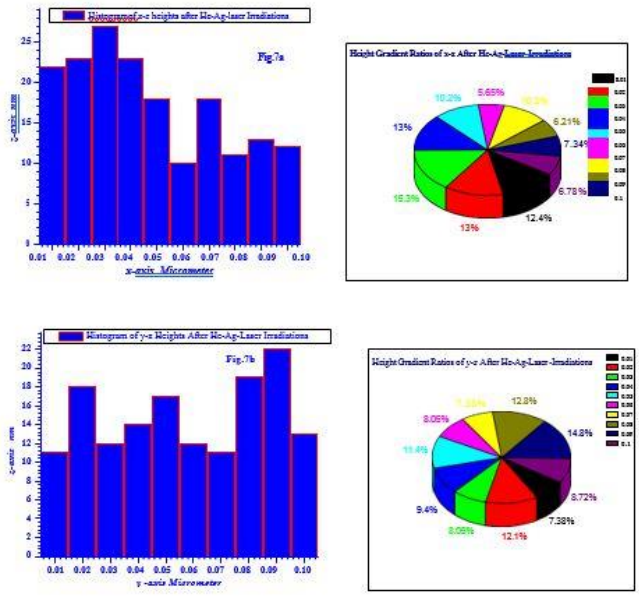

FIG. 7. **2D-AFM histograms with pie charts through (xz, yz) for TiO_2-Assisted *via* Laser/Sonication treatments.**

FIG. 7 is describing heights gradients through xz, yz axes with their pie chart for laser/sonication assisted anatase TiO_2. It can be seen that the fractions of heights are in lower range than pre-treated TiO_2 with heights majority of ~ 10-28 nm. This fact is also confirming our results on the point of view laser/sonication treatments were acting successfully as grains splitter.

Surface area measurements of mesoporous anatase TiO_2

The measurements of BET surface area of both resulted pre-and laser-treated anatase TiO_2 confirmed that the second yield of TiO_2 with advanced technique of laser/sonication treatments gave thermally stable TiO_2 with ultrahigh BET surface area ~789 m^2g^{-1} with average pores sizes ~ 9.2 nm while pre-treated TiO_2 recorded BET surface area ~71 m^2g^{-1} and pores averages of 14.3 nm. This result confirmed the success of ultrahigh energy He-Ag-laser irradiations coupled with sonication as grains sizes splitter (promoter directs to lower sizes).

The present investigations introduced for the 1st time thermally-stable anatase TiO_2 with ultrahigh BET surface area ~ 789 m^2g^{-1} which can be comparable with those reported by Yoshitake et al. who synthesized mesoporous titania with BET surface area over 1200 m^2g^{-1} by using different types of primary amines but their results have reduced by ~ 20% to be stable at 300°C with final record of BET surface area of ~ 500 m^2g^{-1}. On the other hand the present results of laser-treated thermally-stable anatase TiO_2 are better than some of those mentioned in literatures as (TABLE 1). Zhou et al. [25] who were synthesized thermally stable mesoporous TiO_2 anatase with large pores of ~ 10 nm and BET surface area of 122 m^2g^{-1} applying ethylenediamine as phase stabilizer for meso-phase liquid crystal of TiO_2. Otherwise Kim et al. have been synthesized spherical mesoporous TiO_2 by hydrothermal route with pores averages lies in between 5-10.1 nm and BET surface area of 210, 395 m^2g^{-1} calcined at 300,400°C respectively.

TABLE 1. **Calculated BET-specific surface area as function of applied synthesizing techniques for some literatures compared with present article.**

Applied technique	**BET Specific surface area m^2g^{-1}**	**Calcination temperature**
Sol Gel/laser assisted Sol Gel/without laser	789 71	560°C (4 h) 560°C (4 h)
Meso-phase liquid crystal	122	270°C
Hydrothermal/copolymer	210	300°C
Hydrothermal/copolymer	395	400°C
Sol Gel/1° amines	1200	60°C
Sol Gel/1° amines	500	300°C
Sol Gel/NH_4F/HOH	270 138.9	100°C 400°C
Calcination of TiO_2	334 210 125 18	R.T. 523°C 673°C 823°C
Sono chemical method	78.88	R.T.
Microwave method	256	90°C
Chemical vapor deposition/O_2 Jet	123-325	287-320°C

Conclusion

Results obtained confirmed the success of application ultrahigh energy He-Ag-laser irradiations coupled with sonication as splitting agent during growth and nucleation of titanium aggregates making shift to lower particles sizes (8-24 nm). The present investigations have managed to introduce for the 1st time thermally-stable spherical-anatase TiO_2 with ultrahigh BET surface area of ~789 m^2g^{-1} which qualifies this advanced simple technique to be competitive and applied widely.

Acknowledgements

The authors would like to express deep appreciations and thank Administration of Taif-University, Scientific Research Deanship-KSA, for their finance and technical supports for this project under contract number (1438-5508).

REFERENCES

1. Zhao B, Uchikawa K, Wang H. A comparative study of nanoparticles in premixed flames by scanning mobility particle sizer, small angle neutron scattering and transmission electron microscopy. Proceedings of the Combustion Institute. 2007;31(1):851-60.
2. Anpo M, Shima T, Kodama S, et al. Photocatalytic hydrogenation of propyne with water on small-particle titania: Size quantization effects and reaction intermediates. J Phy Chem. 1987;91(16):4305-10.
3. Pratsinis SE. Flame aerosol synthesis of ceramic powders. Progress in Energy and Combustion Science. 1998;24(3):197-219.
4. Wang R, Hashimoto K, Fujishima A, et al. Light-induced amphiphilic surfaces. Nature. 1997;388(6641):431.
5. Li Y, Fan Y, Chen Y. A novel method for preparation of nanocrystalline rutile TiO_2 powders by liquid hydrolysis of $TiCl_4$. J Mat Chem. 2002;12(5):1387-90.
6. Stathatos E, Lianos P, Del Monte F, et al. Formation of TiO_2 nanoparticles in reverse micelles and their deposition as thin films on glass substrates. Langmuir. 1997;13(16):4295-300.
7. Fujishima A, Rao TN, Tryk DA. Titanium dioxide photocatalysis. Journal of Photochemistry and Photobiology C: Photochemistry Reviews. 2000;1(1):1-21.
8. Li W, Guo Y, Zhang P. General strategy to prepare TiO2-core gold-shell nanoparticles as SERS-tags. The Journal of Physical Chemistry C. 2009;114(16):7263-8.
9. Dou B, Dupont V, Pan W, et al. Removal of aqueous toxic Hg (II) by synthesized TiO_2 nanoparticles and TiO_2/montmorillonite. Chemical Eng J. 2011;166(2):631-8.
10. Seo HK, Elliott CM, Shin HS. Mesoporous TiO_2 films fabricated using atmospheric pressure dielectric barrier discharge jet. ACS App Mat Int. 2010;2(12):3397-400.
11. Li W, Gandra N, Ellis ED, et al. pH-Responsive, TiO_2-attached porphyrin for singlet oxygen production in an aqueous solution. ACS App Mat Int. 2009;1(8):1778-84.
12. Park NG, Van de Lagemaat J, Frank AJ. Comparison of dye-sensitized rutile-and anatase-based TiO_2 solar cells. The J Phy Chem. 2000;104(38):8989-94.
13. Innocenzi P, Brusatin G, Babonneau F. Competitive polymerization between organic and inorganic networks in hybrid materials. Chem Mat. 2000;12(12):3726-32.
14. Nagaveni K, Sivalingam G, Hegde MS, et al. Solar photocatalytic degradation of dyes: High activity of combustion synthesized nano TiO_2. App Cat B: Environ. 2004;48(2):83-93.

15. Li W, Gandra N, Courtney SN, et al. Singlet oxygen production upon two-photon excitation of TiO_2 in chloroform. Chem Phys Chem. 2009;10(11):1789-93.
16. Zhang H, Finnegan M, Banfield JF. Preparing single-phase nanocrystalline anatase from amorphous titania with particle sizes tailored by temperature. Nano Letters. 2001;1(2):81-5.
17. Ahn KH, Park YB, Park DW. Kinetic and mechanistic study on the chemical vapor deposition of titanium dioxide thin films by *in situ* FT-IR using TTIP. Surface and Coatings Technology. 2003;171(1-3):198-204.
18. Beattie IR, Gilson TR. Single crystal laser Raman spectroscopy. Proc R Soc Lond A. 1968;307(1491):407-29.
19. Ohsaka T, Izumi F, Fujiki Y. Raman spectrum of anatase, TiO_2. J Raman Spectroscopy. 1978;7(6):321-4.
20. Ohsaka T, Yamaoka S, Shimomura O. Effect of hydrostatic pressure on the Raman spectrum of anatase (TiO_2). Solid State Communications. 1979;30(6):345-7.
21. Maradudin AA, Fein AE. Scattering of neutrons by an anharmonic crystal. Phy Rev. 1962;128(6):2589.
22. Alhuthali A, El-Nahass MM, Atta AA, et al. Study of topological morphology and optical properties of SnO2 thin films deposited by RF sputtering technique. J Lumines. 2015;158:165-71.
23. Elsabawy KM. Synthesis of a tunable MgB 2/Nano-Graphene/MgB 2-Josephson junction-like structure for electronic devices. RSC Adv. 2011;1(6):964-7.
24. Yoshitake H, Sugihara T, Tatsumi T. Preparation of wormhole-like mesoporous TiO_2 with an extremely large surface area and stabilization of its surface by chemical vapor deposition. Chem Mat. 2002;14(3):1023-9.
25. Zhou W, Sun F, Pan K, et al. Well-ordered large-pore mesoporous anatase TiO_2 with remarkably high thermal stability and improved crystallinity: Preparation, characterization and photocatalytic performance. Adv Functional Mat. 2011;21(10):1922-30.
26. Kim DS, Kwak SY. The hydrothermal synthesis of mesoporous TiO_2 with high crystallinity, thermal stability, large surface area and enhanced photocatalytic activity. Applied Catalysis A: General. 2007;323:110-8.
27. Kim DS, Han SJ, Kwak SY. Synthesis and photocatalytic activity of mesoporous TiO_2 with the surface area, crystallite size and pore size. J Colloid and Int Sci. 2007;316(1):85-91.
28. Yu JC, Yu J, Ho W, et al. Effects of F-doping on the photocatalytic activity and microstructures of nanocrystalline TiO_2 powders. Chem Mat. 2002;14(9):3808-16.
29. Arami H, Mazloumi M, Khalifehzadeh R, et al. Sonochemical preparation of TiO_2 nanoparticles. Mat Lett. 2007;61(23-24):4559-61.
30. White LM, Kim MH, Zhang J, et al. A review on synthesis of nano-TiO_2 *via* different methods. Mat Res Bull. 2013;1:6091-8.